

A computational model for exploring particle acceleration during reconnection in macroscale systems

J. F. Drake,¹ H. Arnold,² M. Swisdak,² and J. T. Dahlin³

¹*Department of Physics, the Institute for Physical Science and Technology and the Joint Space Science Institute, University of Maryland, College Park, MD 20742^a*

²*Institute for Research in Electronics and Applied Physics, University of Maryland, College Park, MD 20742*

³*NASA Goddard Space Flight Center code 670, Greenbelt, MD 20771*

A new computational model is presented suitable for exploring the self-consistent production of energetic electrons during magnetic reconnection in macroscale systems. The equations are based on the recent discovery that parallel electric fields are ineffective drivers of energetic particles during reconnection so that the kinetic scales which control the development of such fields can be ordered out of the equations. The resulting equations consist of a magnetohydrodynamic (MHD) backbone with the energetic component represented by macro-particles described by the guiding center equations. Crucially, the energetic component feeds back on the MHD equations so that the total energy of the MHD fluid and the energetic particles is conserved. The equations correctly describe the firehose instability, whose dynamics plays a key role in throttling reconnection and in controlling the spectra of energetic particles. The results of early tests of the model, including the propagation of Alfvén waves in a system with pressure anisotropy and the growth of firehose modes, establish that the basic algorithm is stable and produces reliable physics results in preparation for further benchmarking with particle-in-cell models of reconnection.

^a)Electronic mail: drake@umd.edu

I. INTRODUCTION

Observations of solar flares suggest that a large fraction of the energy released appears as energetic electrons and ions¹⁻³. Solar observations also indicate the highest energy electrons are closest to the inferred position of the x-line⁴. In recent observations of over-the-limb flares the limb of the sun blocked the intense emission from the chromosphere, which enabled direct measurement of the high corona where magnetic energy was released in the flare^{5,6}. The surprise was that a large fraction of the electrons in the high emission region were in the energetic component, indicating that most electrons in the region underwent acceleration. Such observations are consistent with the large number of accelerated electrons seen in flares. Further, the total pressure of these energetic particles was comparable to that of the magnetic field. That energetic electrons can be efficiently produced during reconnection is not limited to flares. In *in situ* satellite measurements in the distant magnetotail energetic electrons in excess of 300 keV were produced. They were broadly peaked around the reconnection x-line rather than localized in boundary layers, suggesting that electrons were able to wander over a broad region⁷.

The observations pose significant challenges to models of electron and ion acceleration during magnetic reconnection. These challenges include: large numbers of electrons undergoing strong heating in flares with the pressure of the energetic component approaching that of the reconnecting magnetic field; the energetic electrons peaking in a broad region around the x-line and not in localized boundary layers; and the particle spectra exhibiting a power law form at high energy.

These observations rule out the classical picture in which reconnection-driven particle acceleration takes place in a boundary layer associated with a single, large-scale reconnection site. Such a single x-line model can not explain the large number of energetic particles produced during reconnection nor their broad spatial distribution. Further, reconnected magnetic field lines release most of their energy as they expand downstream of the x-line rather than in the diffusion regions where the topological change in magnetic structure takes place.

On the other hand, it is also now established that current layers typically spawn multiple magnetic islands in 2D systems^{8,9} or become turbulent due to the generation of multiple x-lines with variable tilt angles in 3D systems¹⁰⁻¹⁴, especially in the presence of strong guide

fields. Observations of flux transfer events (FTEs) at the magnetopause¹⁵, flux ropes in the magnetotail^{16,17} and downflowing blobs during reconnection in the corona^{18,19} support the multi-island, multi-x-line picture of reconnection. That reconnection becomes turbulent is also consistent with recent solar flare observations in which the production of energetic electrons was correlated with the onset of turbulent flows²⁰.

Thus, observations suggest that reconnection-driven particle acceleration takes place in a multi-island or turbulent reconnecting environment rather than in a single, large-scale reconnection site. To understand particle acceleration in such an environment, we write the basic equation for the rate of energy gain of particles in a guiding center system after summing over all particles in a local region

$$\frac{dW}{dt} = E_{\parallel} J_{\parallel} + \frac{P_{\perp}}{B} \left(\frac{\partial B}{\partial t} + \mathbf{v}_E \cdot \nabla B \right) + (P_{\parallel} + np_{\parallel} v_{\parallel}) \mathbf{v}_E \cdot \boldsymbol{\kappa} \quad (1)$$

where W is the total kinetic energy, $\mathbf{v}_E = c\mathbf{E} \times \mathbf{B}/B^2$, v_{\parallel} and p_{\parallel} are the bulk parallel velocity and momentum, and the curvature is $\boldsymbol{\kappa} = \mathbf{b} \cdot \nabla \mathbf{b}$ with \mathbf{b} the unit vector along \mathbf{B} . The parallel and perpendicular pressures are P_{\parallel} and P_{\perp} and n is the density. The equations apply to any species for which the guiding-center approximation is valid. However, for ions an additional term, the dot product of the polarization drift into the electric field, is required since the kinetic energy associated with the $\mathbf{E} \times \mathbf{B}$ drift is not negligible. The first term in Eq. (1) is the acceleration by the parallel electric field. The second term corresponds to perpendicular heating or cooling due to the conservation of the magnetic moment μ (Betatron acceleration). The third term drives parallel acceleration and arises from the first-order Fermi mechanism^{21–23}. Freshly reconnected field lines downstream from a reconnecting x-line accelerate as a result of the tension force that causes them to “straighten”. Particles that reflect from this moving field line receive a Fermi “kick” and thereby gain energy.

Betatron acceleration is typically not important during reconnection since the release of magnetic energy leads to a reduction of B and therefore the perpendicular temperature²⁴. Depending on the strength of the ambient guide magnetic field either E_{\parallel} or Fermi reflection dominates electron heating during reconnection. Fermi reflection dominates for weak to modest guide fields while E_{\parallel} dominates for large guide fields. A recent important discovery is that energetic electron production plunges in the strong guide field limit where E_{\parallel} dominates and therefore E_{\parallel} is an inefficient driver of energetic particles^{14,25}. This result also suggests that high frequency waves, such as double layers and electron solitary waves, which have

been identified in both observations and simulations of reconnection²⁶, are not a major driver of energetic electrons during reconnection. Importantly, in a regime where Fermi reflection dominates particle energy gain and magnetic energy release are directly linked (consistent with flare observations)^{8,27}, energetic particles spread over broad regions and are not localized in boundary layers^{13,14}, and large numbers of particles undergo acceleration.

Energetic particle spectra in heliospheric observations typically take the form of powerlaws. On the other hand, the particle spectra in PIC simulations of reconnection in the non-relativistic regime (Alfvén speed much smaller than the velocity of light) typically do not form powerlaws^{14,24} except in the limit in which the upstream plasma pressure is much lower than that of the magnetic field (extremely low plasma β)²⁸. Simple “particle-in-a-box” models in which energy drive and loss mechanisms are included exhibit powerlaw spectra^{27,29}. The hardest spectra from such models have distribution functions f that scale as v^{-5} , which correspond to the upper limit so that the integrated particle energy remains finite. The particle fluxes at this limit scale as $\varepsilon^{-1.5}$ with ε the particle energy. Electron fluxes that scale as $\varepsilon^{-1.5}$ have been observed in solar flares³⁰. Ion fluxes typically scale as $\varepsilon^{-1.5}$ in the solar wind³¹ and in the outer heliosphere^{32,33}. Thus, simulations of reconnection-driven particle acceleration that are large enough to include realistic loss mechanisms appear to be required to explain observations.

The fundamental question is how to explore particle acceleration in macro-scale reconnecting systems such as the solar corona where the separation between kinetic scales and macro-scales approaches 10^{10} (the Debye length is less than a centimeter for $n \sim 10^{10}/\text{cm}^3$ and $T_e \sim 100\text{eV}$ while macro-scales approach 10^4km). The development of Parker-like transport equations that describe reconnection-driven particle acceleration illuminate the important physical processes that control spectra (pressure anisotropy, feedback on the Fermi drive, particle loss versus energy gain times)^{27,34–36}. They also yield guidelines on the range of spectral indices that are possible in reconnecting systems. As discussed previously, in non-relativistic reconnection, the spectral index of the energetic particles can not fall below 1.5²⁷. However, such models are not able to directly describe the reconnection dynamics of a given event such as an impulsive flare in the sun’s atmosphere even when they are paired with the MHD description of the system – scattering in such models is assumed to be strong enough so that the energetic particles are tied to the local fluid and so are unable to stream along ambient magnetic field³⁶. Such strong scattering, however, is inconsistent with solar

flare observations³⁷.

Exploring the dynamics of test particles in the MHD fields produces useful information about how particles gain energy^{38–41}. However, the energy going into the energetic particles can run away since there is no feedback on the MHD fields. It is also possible to embed PIC models into large-scale MHD descriptions at selected locations where reconnection takes place⁴². However, such models presume that particle energy gain is highly localized in space around isolated x-lines, which is not consistent with the description of particle energy gain during the development and interaction of macro-scale magnetic islands or the development of turbulence in large-scale current layers.

The problem with conventional PIC codes in the context of modeling large-scale systems is that the Debye length has to be resolved to avoid non-physical heating of the electron macro-particles. Implicit PIC models avoid this constraint but still need to resolve the electron and ion inertial scales⁴³. Conventional hybrid codes (fluid electrons and macro-particle ions) can not model electron acceleration and must still resolve the ion inertial scale and the ion Larmor radius and therefore can not be used to explore energetic particle spectra in macroscale systems.

The fundamental question is whether kinetic scale boundary layers play an essential role in the development of particle energy gain during impulsive flares in macro-scale systems such the sun’s corona. The rate of reconnection in kinetic descriptions corresponds to inflows that are around $0.1V_A$ where V_A is the Alfvén speed based on the upstream reconnecting magnetic field^{44–46}. On the other hand, MHD descriptions of reconnection at low resistivity generate multiple magnetic islands and yield reconnection rates that, while somewhat slower than in kinetic models, are, nevertheless, insensitive to plasma resistivity^{47–49}. The inclusion of current-driven resistivity can boost MHD reconnection rates to values comparable to kinetic models. Kinetic boundary layers control the regions where E_{\parallel} is non-zero^{50,51}. However, it is Fermi reflection and not E_{\parallel} that is the dominant driver of energetic particles. Particle energy gain from Fermi reflection takes place over macro-scale regions where magnetic fields are releasing energy and takes place even where $E_{\parallel} = 0$. Physically, particles moving along bent field lines have curvature drifts along the reconnection electric field and therefore gain energy as long as $\boldsymbol{\kappa} \cdot \mathbf{v}_E$ is positive (see Eq. (1)). The conclusion therefore is that including kinetic-scale boundary layers is not required to describe the dynamics of energy gain of the most energetic particles in macroscale systems. The MHD model is a reasonable description

of heating during magnetic reconnection – either through the formation of switch-off slow shocks in anti-parallel reconnection or a combination of rotational discontinuities and slow shocks in the case of reconnection with a guide field⁵².

We conclude therefore that we can explore particle acceleration during magnetic reconnection in macroscale systems without resolving the kinetic scale boundary layers that limit traditional kinetic models. Here we present a novel computational model that combines the MHD description of the plasma dynamics with a macroparticle description but in which all kinetic scales are ordered out of the system of equations. The macro-particles can be small in number density but can contribute a pressure that can be comparable to the pressure of the reconnecting magnetic field. They move within the MHD grid and are advanced in parallel with the fluid equations using the guiding center equations based on the MHD electric and magnetic fields. The particles feed back on the MHD fluid through their pressure-driven $\mathbf{J}_h \times \mathbf{B}$ force. The entire system conserves the total energy, including that of the MHD fluid (ions and the bulk electrons), the magnetic field and the kinetic energy of the macroparticles. In the early phase of exploration of this model, we are treating only electrons as macroparticles but the ions can also be similarly treated.

There have been earlier efforts to couple the MHD equations to a gyro-kinetic model for studying the stability of Alfvén waves⁵³ and the internal kink mode in tokamaks⁵⁴. However, the gyrokinetic model orders out Fermi reflection, which for exploring particle acceleration during reconnection is essential. The basic ordering that we adopt is consistent with that discussed by Kulsrud in which Fermi reflection is retained⁵⁵. Overall energy conservation was not discussed in this previous work. Others have coupled the MHD equations to a general kinetic particle description⁵⁶. The importance and challenge of producing a set of equations that conserves energy exactly has been discussed previously⁵⁷.

In Sec. II we present the basic equations and discuss how the energetic component feeds back on the MHD fluid, leading to a set of equations in which total energy is conserved. In Sec. III we show the results of early tests of the code on Alfvén wave propagation in a system with a finite pressure anisotropy and firehose instability that demonstrate that there are no fundamental computational problems associated with implementing such a model.

II. BASIC EQUATIONS AND CONSERVATION PROPERTIES

We treat a system with three distinct classes of particles: ions of density n and temperature T_i , cold electrons with density n_c and temperature T_c and energetic electrons with density $n_h = n - n_c$. The hot electrons will be treated as macro-particles that are evolved through the MHD grid by the guiding center equations. Momentum equations can be written down for each of the three species, the ions

$$m_i n \frac{d\mathbf{v}_i}{dt} = n e \mathbf{E} + \frac{n e}{c} \mathbf{v}_i \times \mathbf{B} - \nabla P_i, \quad (2)$$

the cold electrons

$$m_e n_{ec} \frac{d\mathbf{v}_{ec}}{dt} = -n_{ec} e \mathbf{E} - \frac{n_{ec} e}{c} \mathbf{v}_{ec} \times \mathbf{B} - \nabla P_{ec}, \quad (3)$$

and the hot electrons

$$\frac{\partial(n_{eh} \bar{\mathbf{p}}_{eh})}{\partial t} = -n_{eh} e \mathbf{E} - \frac{n_{eh} e}{c} \bar{\mathbf{v}}_{eh} \times \mathbf{B} - \nabla \cdot \mathbb{T}_{eh}. \quad (4)$$

\mathbf{v}_i , \mathbf{v}_{ec} and $\bar{\mathbf{v}}_{eh}$ are the ion and electron cold and hot velocities and $\bar{\mathbf{p}}_{eh}$ is the average hot electron momentum (an average of the local momenta of individual particles). The hot electron stress tensor \mathbb{T}_{eh} includes both the pressure and convective derivatives and as a consequence the inertia term in Eq. (4) does not include the convective derivative. The hot electron stress tensor is given by

$$\mathbb{T}_{eh} = \int d\mathbf{p}_e \frac{\mathbf{p}_e \mathbf{p}_e}{\gamma_e} f \quad (5)$$

with \mathbf{p}_e the hot electron momentum with distribution f and γ_e is the relativistic Lorentz factor. The form of \mathbb{T}_{eh} for guiding center particles and the reason for writing the hot electron momentum equation in this form will be clarified later. These equations are formally exact if there are mechanisms for maintaining the isotropy of P_i and P_{ec} . The usual challenge in deriving the MHD equations from the multi-fluid equations is that the electric field and Lorentz force terms are formally larger than the other terms in the equations. In Eq. (2), for example, taking $v_i \sim V_A$ and $d/dt \sim V_A/L$, the inertia term is of order $d_i/L \ll 1$ and therefore small if the ion inertial length $d_i = V_A/\Omega_i$ is much smaller than the system scale length L . The usual procedure is then to sum the two fluid equations or in the present case the three fluid equations, which eliminates the electric field completely and reduces the Lorentz forces to the $\mathbf{J} \times \mathbf{B}/c$ force of the usual MHD equation. Since $J \sim cB/4\pi L \sim neV_A(d_i/L) \ll neV_A$, the inertial and $\mathbf{J} \times \mathbf{B}$ terms in the MHD equations are the same order.

In the present system we carry out the same procedure while discarding the electron inertial terms, which are small as long as $L \gg d_e$ with d_e the electron inertial length. We emphasize that we are discarding only the inertia of the bulk flow associated with the hot electrons and not the inertia associated with individual hot electrons. The dominant motion of individual hot electrons in the guiding center limit is parallel to the ambient magnetic field. The perpendicular motion arises from \mathbf{v}_E with the various perpendicular gradient drifts being much smaller. The large parallel velocities of the hot electrons largely cancel when summed to produce a large parallel pressure but not a large streaming velocity. Because we are discarding the electron fluid inertia, in summing the three momentum equations we also discard the parallel electric field and the parallel pressure gradient of the hot electrons. The hot electrons are unable to couple to the MHD fluid along the ambient magnetic field through their parallel pressure gradient. Their parallel motion is instead controlled by the inertia of individual particles and electromagnetic forces. They act only on the MHD fluid through their forces perpendicular to \mathbf{B} . An extension of such a model to include a finite macroscale parallel electric field is discussed at the end of the paper. Thus, summing the three momentum equations yields

$$\rho \frac{d\mathbf{v}}{dt} = \frac{1}{c} \mathbf{J} \times \mathbf{B} - \nabla P - (\nabla \cdot \mathbb{T}_{eh})_{\perp}, \quad (6)$$

where we have suppressed the subscript so that \mathbf{v} is the fluid velocity with mass density ρ and $P = P_i + P_{ec}$. The energetic particles act on the MHD fluid through their stress tensor. It is convenient, however, to express this force in terms of the hot electron current $\mathbf{J}_{ehT\perp}$ driven by the stress tensor. This current is obtained from the hot electron momentum equation by first subtracting the dominant current associated with \mathbf{v}_E (which cancels that of the ions and cold electrons) from \mathbf{J}_{eh} . This yields

$$\mathbf{J}_{ehT\perp} = \frac{c}{B} \mathbf{b} \times \nabla \cdot \mathbb{T}_{eh} \quad (7)$$

We now proceed to simplify the form of \mathbb{T}_{eh} for guiding center electrons. The stress tensor can be written in two distinct components associated with the averaged hot electron convection and the pressure. In the direction perpendicular to \mathbf{B} , the dominant perpendicular motion of the hot electrons is given by \mathbf{v}_E with other drifts being smaller in the ratio of the Larmor radius to the macroscale L . For $v_E \sim V_A$ the inertia associated with this perpendicular motion is negligible as long as $m_e/m_i \ll \beta_{eh\perp} \sim 1$. In this limit the stress tensor takes the

usual gyrotropic form

$$\mathbb{T}_{eh} = T_{eh\parallel} \mathbf{b}\mathbf{b} + P_{eh\perp} (\mathbb{I} - \mathbf{b}\mathbf{b}), \quad (8)$$

where \mathbb{I} is the unit tensor, $T_{eh\parallel}$ is the stress tensor along the magnetic field \mathbf{B} and $P_{eh\perp}$ is the usual perpendicular pressure,

$$P_{eh\perp} = \int d\mathbf{p}_e \frac{p_{e\perp}^2}{\gamma_e} f, \quad (9)$$

where in the frame drifting with \mathbf{v}_E , $f = f(\mathbf{x}, p_{e\parallel}, p_{e\perp}, t)$ since there is no other mean drift perpendicular to \mathbf{B} . $T_{eh\parallel}$ includes the mean parallel drifts of the hot electrons and can be written as a combination of the usual parallel pressure $P_{eh\parallel}$ plus the mean parallel convection terms,

$$T_{eh\parallel} = \int d\mathbf{p}_e \frac{p_{e\parallel}^2}{\gamma_e} f = P_{eh\parallel} + n_{eh} \bar{p}_{eh\parallel} \bar{v}_{eh\parallel} \quad (10)$$

with

$$P_{eh\parallel} = \int d\mathbf{p}_e (p_{e\parallel} - \bar{p}_{eh\parallel}) \left(\frac{p_{e\parallel}}{\gamma_e} - \bar{v}_{eh\parallel} \right) f. \quad (11)$$

The hot electron parallel bulk streaming terms in Eq. (10) are nominally much smaller than the parallel pressure since

$$n_h \bar{p}_{eh\parallel} \bar{v}_{eh\parallel} \sim \frac{m_e J_{\parallel}^2}{n e^2} \sim \frac{B^2}{4\pi} \frac{d_e^2}{L^2} \sim P_{eh\parallel} \frac{d_e^2}{L^2} \ll P_{eh\parallel}. \quad (12)$$

On the other hand, we demonstrate below that exact energy conservation requires that this nominally small contribution to $T_{eh\parallel}$ be retained since these contributions appear in the expression for electron energy gain given in Eq. (1). With the form of the stress tensor given in Eq. (8), the hot electron current can be expressed as⁵⁸

$$\mathbf{J}_{ehT\perp} = \frac{c}{B} (T_{eh\parallel} - P_{eh\perp}) \mathbf{b} \times \boldsymbol{\kappa} + \frac{c}{B} \mathbf{b} \times \nabla P_{eh\perp}. \quad (13)$$

An equivalent form for the hot electron current is

$$\mathbf{J}_{ehT\perp} = \frac{c}{B} \mathbf{b} \times (P_{eh\perp} \nabla \ln(B) + T_{eh\parallel} \boldsymbol{\kappa}) - c \left(\nabla \times \frac{P_{eh\perp} \mathbf{b}}{B} \right)_{\perp}, \quad (14)$$

where the first term on the right is the gradient B drift, the second is the curvature drift and the third is the magnetization current⁵⁹. The MHD equation with energetic electron feedback can then be written as

$$\rho \frac{d\mathbf{v}}{dt} = \frac{1}{c} \mathbf{J} \times \mathbf{B} - \nabla P - \frac{1}{c} \mathbf{J}_{ehT\perp} \times \mathbf{B}. \quad (15)$$

The calculations leading to Ohm's law in this three species system parallel that of the electron-ion system. As discussed previously, the dominant terms in Eqs. (3)-(4) are the electric field and Lorentz terms. Adding the two electron equations and discarding the pressures and stress tensor, we obtain

$$\mathbf{E} = \frac{1}{nc}(n_{ec}\mathbf{v}_{ec} + n_{eh}\mathbf{v}_{eh}) \times \mathbf{B} = \frac{1}{nec}\mathbf{J} \times \mathbf{B} - \frac{1}{c}\mathbf{v} \times \mathbf{B} \simeq -\frac{1}{c}\mathbf{v} \times \mathbf{B}, \quad (16)$$

where we have added and subtracted $n\mathbf{v}$ in the Lorentz force and again used the fact that $J \ll nev$ to eliminate the $\mathbf{J} \times \mathbf{B}$ or Hall term in Ohm's law. Thus, Ohm's law, which determines \mathbf{E} in terms of \mathbf{v} is unchanged from the usual MHD prescription. The equations for the pressure P and mass density ρ are also unchanged.

The model is completed by the guiding-center equations for the hot electrons⁶⁰

$$\frac{d}{dt}p_{e\parallel} = p_{e\parallel}\mathbf{v}_E \cdot \boldsymbol{\kappa} - \frac{\mu_e}{\gamma_e}\mathbf{b} \cdot \nabla B \quad (17)$$

with $p_{e\parallel}$ the parallel momentum of a macroparticle electron with its magnetic moment given by

$$\mu_e = p_{e\perp}^2/2B. \quad (18)$$

$p_{e\perp}$ is determined from the conservation of μ_e . The particle velocity is given by \mathbf{v}_E and the parallel streaming $v_{eh\parallel} = p_{eh\parallel}/(\gamma_e m_e)$ along \mathbf{B} , the curvature and gradient B drifts being smaller in the ratio of the Larmor radius to the macroscale L . The ordering of the hot electron drifts and their energy gain in Eqs. (17)-(18) are equivalent to Kulsrud's guiding center description⁵⁵. A critical goal in developing a credible set of equations to describe particle acceleration is to establish energy conservation. By taking the dot product of Eq. (15) with \mathbf{v} and integrating over space the energy conservation relation takes the form

$$\frac{d}{dt}W_{MHD} = - \int d\mathbf{x} \mathbf{J}_h \cdot \mathbf{E} = -\frac{d}{dt}W_h = - \int d\mathbf{x} \left[T_{eh\parallel}\mathbf{v}_E \cdot \boldsymbol{\kappa} + \frac{P_{eh\perp}}{B} \left(\frac{\partial B}{\partial t} + \mathbf{v}_E \cdot \nabla B \right) \right] \quad (19)$$

where W_{MHD} is the usual energy in the MHD description, including the kinetic energy of the bulk flow, the thermal energy and magnetic energy. dW_h/dt is the rate of change of the energy of the hot electrons. dW_h/dt in Eq. (19) is equal to the spatial integral of the rate of energy gain in Eq. (1). We again note that the convective terms in the curvature in Eq. (19) are nominally small since $d_e^2/L^2 \ll 1$ but must be retained so that the energy gain in Eq. (1), which follows from Eq. (17) and the conservation of μ_e , matches that in Eq. (19). Having equations that exactly conserve energy facilitates testing the model and is desirable⁵⁷.

The equations presented above provide a complete self-consistent system for exploring the production of energetic electrons in macroscale systems. Since the electrons are evolved in the fields from the MHD equations, the artificial heating associated with the PIC model when the Debye length is not resolved is not an issue. Similar equations can be written down that also include energetic ions although the neglect of their inertia requires that their number density be small. Beyond energy conservation, an important consideration is whether the equations properly describe the feedback of the energetic component on the MHD fluid. It is straightforward to show that the inclusion of an ambient pressure anisotropy in the hot component through \mathbb{T}_{eh} yields the correct firehose stability criterion. In the case of magnetic reconnection the firehose stability boundary plays an important role in throttling reconnection^{22,23} and in controlling the spectral index of the energetic particles resulting from reconnection²⁷. The firehose stability boundary will act similarly in this model if the pressure in the energetic component is too high. With these equations the production of energetic particles in realistic macroscale systems can be explored where realistic losses can be included and the realistic spectra of synchrotron emission from the volume and Bremsstrahlung emission at system boundaries can be calculated for direct comparison with X-ray observations from satellite missions such as Ramaty High Energy Solar Spectroscopic Imager (RHESSI) and ground-based radio observatories such as the Nobeyama Radioheliograph (NoRH)⁶¹ or the Extended Owens Valley Solar Array (EOVSA)⁶².

III. TESTS OF THE *KGLOBAL* MODEL

As discussed in the previous section, the pressure anisotropy of the energetic electrons plays an important role in throttling magnetic reconnection and limiting the energy gain of those particles^{22,23,27}. Thus to ensure the model correctly describes the impact of pressure anisotropy on magnetic field dynamics we benchmark the code with two simple wave modes that are evolved in a system with an imposed initial pressure anisotropy: the linear propagation of stable, circularly polarized Alfvén waves; and the linear growth of firehose modes. The correct solutions of both of these tests are, of course, well known⁶³.

The new computational model was constructed by merging the fluid evolution equations of the *f3D* code⁶⁴ (with the Hall terms in Ohm’s law removed) and the particle treatment in the *p3d* code⁶⁵, modified to step the particles in the guiding center limit. Time stepping is

with a second order trapezoidal leapfrog scheme with a fourth order viscosity added to each of the fluid equations to prevent the buildup of noise at the grid scale.

In this new model the magnetic field strength, B_0 , and density, n_0 , define the Alfvén speed, $V_A = \sqrt{B_0^2/4\pi m_i n_0}$. Since there are no kinetic scales that enter the equations, lengths and times are normalized to a macroscale length, L , and Alfvén crossing time, $\tau_A = L/V_A$. This normalization allows us to set the physical distance of the longest dimension in our simulations to $2\pi L$ where L can be any macroscopic scale length. Electric fields and temperatures are normalized to $V_A B_0/c$ and $m_i V_A^2$, respectively. A fourth order hyperviscosity, $\nu \nabla^4$, is included for every quantity evolved on the grid (magnetic field, ion density, momentum and pressure and cold electron pressure).

The tests were carried out in a system with two space dimensions with $B_x = B_0$. The ion to hot electron mass ratio is set to 25 (the cold electrons are massless). For a given hot electron pressure and density the mass ratio controls the streaming velocity of electrons through the system. For linear waves with an imposed initial pressure anisotropy the evolution of the pressure does not enter the equations so the value of electron mass does not influence the dynamics. The temperature of the ions and the cold electrons was 1/12. For the hot electrons, the temperature was varied to control the magnitude of the anisotropy of their pressure tensor. The box size was varied from 256 x 64 cells to 512 x 256 cells and there were 160-320 particles per grid cell.

In the first benchmark of the model we propagated a circularly-polarized Alfvén wave along a magnetic field in a system with an imposed hot electron pressure anisotropy. We initialized the simulations with a perturbation with a wavelength equal to the size of the box. After propagating the wave for a time τ_A , we measured its speed. Our equations yield the phase speed V_p of an Alfvén wave:

$$V_p = V_A \sqrt{1 - 4\pi \frac{P_{\parallel} - P_{\perp}}{B^2}} \equiv V_A \alpha, \quad (20)$$

where $\alpha = \sqrt{1 - 4\pi(P_{\parallel} - P_{\perp})/B^2}$. This result is identical to that from the CGL equations since in the linear limit of the system the pressure remains unperturbed. In Figure 1 the wave phase speed V_p is plotted as a function of the anisotropy parameter α . The agreement with linear wave theory is excellent.

In our second benchmark we explored the linear growth of the firehose instability with an imposed initial unstable pressure anisotropy with $\alpha^2 = -0.16$. We initialized the simulation

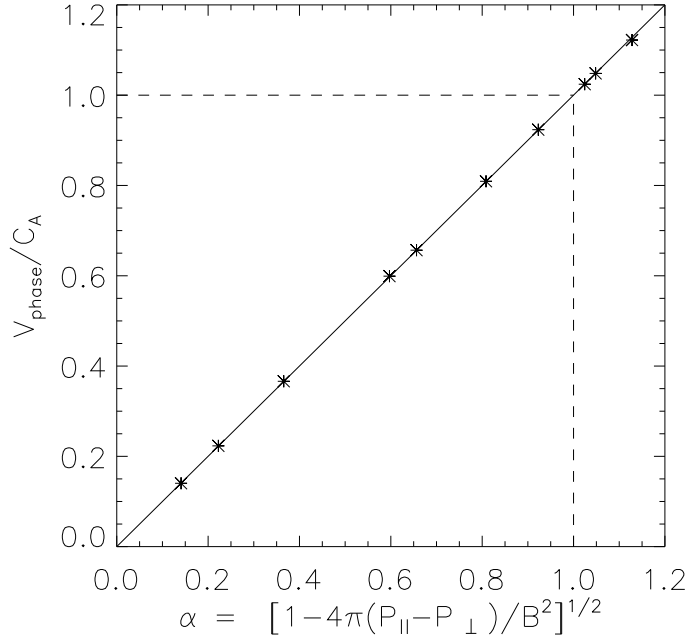


FIG. 1. For each of ten simulations we plot the measured phase speed of the Alfvén wave V_p versus the anisotropy parameter α . The solid line is what we expect from our model, which is the same as that of the linearized CGL equations. The dotted lines show where the isotropic Alfvén wave lies and separates the region where P_{\parallel} is greater than P_{\perp} from where it is smaller.

with small sinusoidal perturbations for 18 values of the wavenumber, $k = m/2\pi L$, where $m = 1, 2, \dots$ is the mode number, and the viscosity was $\nu = 6.0 \cdot 10^{-5}$. The theoretical growth rate is given by $\gamma = kV_A|\alpha| - \nu k^4$. The viscosity controls the cutoff of the instability at short spatial scales. In Figure 2 we plot the theoretical (solid red line) and numerical growth rates (black stars) for the range of unstable wave numbers. For $m > 18$ the modes are stable. There is excellent agreement between the new model and what one would expect from linear theory.

IV. SUMMARY AND DISCUSSION

The enormous separation between kinetic scales (the Debye length, the electron and ion inertial scales and Larmor radii) in the solar corona (as small as a centimeter) and the energy release scales (10^4 km), mean that modeling the release of energy in flares in the solar corona and other astrophysical systems using a PIC model, which needs to resolve the Debye scale,

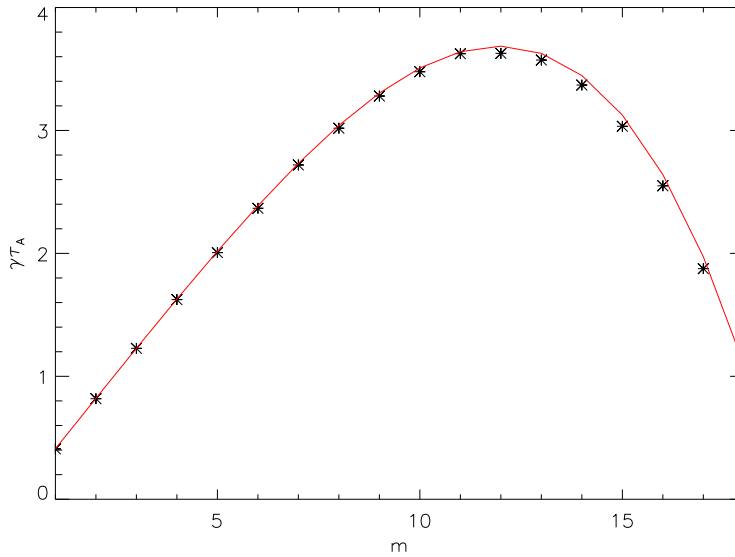


FIG. 2. Normalized growth rate, $\gamma\tau_A$, versus the mode number, $m = 2\pi kL$, for a range of unstable values of m . The numerically determined values of $\gamma\tau_A$ are marked with black stars and the theoretical growth rate as a red line.

is not feasible even with projected increases in computational power. Recent advances in our understanding of the mechanisms for particle acceleration^{13,14}, suggest that these boundary layers, which control the structure of parallel electric fields, play only a minor role in the production of the most energetic particles. Particle acceleration is controlled by the large-scale dynamics of magnetic fields through the merging of magnetic islands in 2D systems and the turbulent interactions of x-lines in the more physically realistic 3D systems. We have presented here a new model in which we have ordered out all of the relevant kinetic boundary layers. The result is a model that is scale independent and therefore capable of modeling macroscale systems.

The model consists of an MHD backbone in which macroparticles (electrons) move through the MHD grid using the guiding center equations with electric and magnetic fields given by the usual MHD prescription. Importantly, the energetic electrons feed back on the MHD fluid through the perpendicular currents associated with their anisotropic stress tensor. The consequence is that energy is conserved exactly. Further the development of pressure anisotropy of the energetic component (with $P_{\parallel} > P_{\perp}$) properly describes the reduction in magnetic tension that drives reconnection and therefore controls the feedback of

the energetic particles on the dynamics of reconnection. The equations describing the full system consist of Eqns. (8)-(18) with the energy conservation relation given in Eqn. (19). A code has been developed to solve these equations by merging the basic algorithms of the *f3D* Hall MHD and *p3d* PIC codes. The resulting model has been benchmarked with the propagation of Alfvén waves and firehose modes in a system with a specified initial pressure anisotropy.

Our plans are to proceed with the exploration of electron heating and acceleration in a simple 2D reconnecting system. There are a variety of simulation results already in the literature on the scaling of reconnection-driven, electron heating with the upstream parameters of the system^{66,67}. The results of these simulations can be compared with the results from the present model.

Before carrying out these reconnection simulations, however, we plan to carry out an upgrade of the model to include a large-scale parallel electric field. We have argued that the parallel electric fields that develop in the boundary layers that form during reconnection are not important for the production of the most energetic particles since these boundary layers occupy very little volume in a macroscale system – their widths scale with the electron skin depth. However, it has now been established that large-scale, parallel electric fields can develop as a result of electron pressure gradients in reconnecting systems⁶⁷⁻⁶⁹. Both electrons and ions are heated as they enter the reconnection exhaust. Because the thermal motion of electrons is so much greater than that of the ions, especially for mass-ratios that approach realistic values, electrons try to escape on the reconnected field lines threading the exhaust, which extend into the upstream plasma that has not yet entered the exhaust. Charge neutrality, of course, prevents the electrons from streaming upstream and the result is a parallel potential that traps electrons in the exhaust. This potential is not large enough to significantly impact the most energetic electrons in the system. However, electrons that first enter the exhaust drop down the potential and boost their parallel velocity. This energy increase facilitates subsequent energy gain through Fermi reflection^{67,69}. The parallel electric field associated with the charge neutrality constraint can be calculated from the electron parallel force balance, obtained from the sum of the electron momentum equations ((3) and (4)) projected along the magnetic field direction with the total inertia of the electrons

neglected⁶⁷. The resulting expression for E_{\parallel} is given by

$$E_{\parallel} = -\frac{1}{ne} (\mathbf{b} \cdot \nabla P_{ec} + \mathbf{b} \cdot (\nabla \cdot \mathbb{T}_{eh})). \quad (21)$$

Note that the individual streaming velocities of the cold and hot electrons and their associated inertias could be large but the constraint on the total parallel current requires that the sum of the streaming velocities be small. This is a traditional return current picture in which hot electrons stream outwards from a region where magnetic energy is being released but drive a return current of cold electrons that eliminates the net electron current and prevents charge separation of the two species. The physics argument leading to Eq. (21) is similar to that presented by Kulsrud to calculate E_{\parallel} ⁵⁵. He argued that the parallel electric field would develop to maintain charge neutrality in the system. His expression for E_{\parallel} includes corrections associated with ion dynamics, which are of order m_e/m_i smaller than those retained in Eq. (21). In our model the Debye length is ordered out so the system must remain charge neutral. The ion density is calculated with a standard continuity equation with a velocity given by the MHD momentum equation. The energetic electron density is calculated by mapping the energetic electrons onto the MHD grid with an appropriate interpolation scheme. The cold electron density is then calculated by requiring that the sum of the cold and hot electron densities match that of the ions. The physics leading to charge neutrality is the strong parallel motion of the cold electrons that fills in for the hot electrons motion along the ambient magnetic field.

Thus, our goal is to extend the present model by incorporating the parallel electric field into the equations and then to proceed with a comparison of electron heating in simple 2D reconnecting systems using the new model and standard PIC.

V. ACKNOWLEDGEMENTS

This work has been supported by NSF Grant Nos. PHY1805829 and PHY1500460, NASA Grant Nos. NNX14AC78G and NNX17AG27G and the FIELDS team of the Parker Solar Probe (NASA contract NNN06AA01C). J.T.D. acknowledges support from the NASA LWS Jack Eddy Fellowship administered by the University Corporation for Atmospheric Research in Boulder, Colorado. Simulations were carried out at the National Energy Research Scientific Computing Center. We acknowledge informative discussions with Dr. William

Daughton, Prof. A. B. Hassam and Dr. G. Hammett. Simulation data is available on request.

REFERENCES

- ¹R. P. Lin and H. S. Hudson, *Sol. Phys.* **17**, 412 (1971).
- ²A. G. Emslie, H. Kucharek, B. R. Dennis, N. Gopalswamy, G. D. Holman, G. H. Share, A. Vourlidas, T. G. Forbes, P. T. Gallagher, G. M. Mason, T. R. Metcalf, R. A. Mewaldt, R. J. Murphy, R. A. Schwartz, and T. H. Zurbuchen, *Journal of Geophysical Research (Space Physics)* **109**, A10104 (2004).
- ³A. G. Emslie, B. R. Dennis, G. D. Holman, and H. S. Hudson, *J. Geophys. Res.* **110**, A11103 (2005).
- ⁴L. Sui and G. D. Holman, *Astrophys. J.* **596**, L251 (2003).
- ⁵S. Krucker, H. S. Hudson, S. M. White, S. Masuda, J.-P. Wuelser, and R. P. Lin, *ApJ* **714**, 1108 (2010).
- ⁶M. Oka, S. Ishikawa, P. Saint-Hilaire, S. Krucker, and R. P. Lin, *ApJ* **764**, 6 (2013), arXiv:1212.2579 [astro-ph.SR].
- ⁷M. Øieroset, R. P. Lin, T. D. Phan, D. E. Larson, and S. D. Bale, *Phys. Rev. Lett.* **89**, 195001 (2002).
- ⁸J. F. Drake, M. Swisdak, K. M. Schoeffler, B. N. Rogers, and S. Kobayashi, *Geophys. Res. Lett.* **33**, 13105 (2006).
- ⁹R. L. Fermo, J. F. Drake, and M. Swisdak, *Phys. Rev. Lett.* **108**, 255005 (2012).
- ¹⁰R. Schreier, M. Swisdak, J. F. Drake, and P. A. Cassak, *Phys. Plasmas* **17**, 110704 (2010).
- ¹¹W. Daughton, V. Roytershteyn, H. K. and L. Yin, B. J. Albright, B. Bergen, and K. J. Bowers, *Nature Phys.* **7**, 539 (2011).
- ¹²Y.-H. Liu, W. Daughton, H. Karimabadi, H. Li, and V. Roytershteyn, *Physical Review Letters* **110**, 265004 (2013).
- ¹³J. T. Dahlin, J. F. Drake, and M. Swisdak, *Phys. Plasmas* **22**, 100704 (2015), arXiv:1503.02218 [physics.plasm-ph].
- ¹⁴J. T. Dahlin, J. F. Drake, and M. Swisdak, *Physics of Plasmas* **24**, 092110 (2017), arXiv:1706.00481 [physics.plasm-ph].
- ¹⁵C. T. Russell and R. C. Elphic, *Space Science Rev.* **22**, 681 (1978).

- ¹⁶J. A. Slavin, R. P. Lepping, J. Gjerloev, D. H. Fairfield, M. Hesse, C. J. Owen, M. B. Moldwin, T. Nagai, A. Ieda, and T. Mukai, *Journal of Geophysical Research (Space Physics)* **108**, 1015 (2003).
- ¹⁷L.-J. Chen, A. Bhattacharjee, P. A. Puhl-Quinn, H. Yang, N. Bessho, S. Imada, S. Muhlbachler, P. W. Daly, B. Lefebvre, Y. Khotyaintsev, A. Vaivads, A. Fazakerley, and E. Georgescu, *Nature Phys.* **4**, 19 (2008).
- ¹⁸D. E. McKenzie and H. S. Hudson, *ApJ Lett.* **519**, L93 (1999).
- ¹⁹S. L. Savage and D. E. McKenzie, *ApJ* **730**, 98 (2011).
- ²⁰E. P. Kontar, J. E. Perez, L. K. Harra, A. A. Kuznetsov, A. G. Emslie, N. L. S. Jeffrey, N. H. Bian, and B. R. Dennis, *Physical Review Letters* **118**, 155101 (2017), arXiv:1703.02392 [astro-ph.SR].
- ²¹B. Kliem, *ApJ* **90**, 719 (1994).
- ²²J. F. Drake, M. Swisdak, H. Che, and M. A. Shay, *Nature* **443**, 553 (2006).
- ²³J. F. Drake, M. Opher, M. Swisdak, and J. N. Chamoun, *ApJ* **709**, 963 (2010).
- ²⁴J. T. Dahlin, J. F. Drake, and M. Swisdak, *Physics of Plasmas* **21**, 092304 (2014), arXiv:1406.0831 [physics.plasm-ph].
- ²⁵J. T. Dahlin, J. F. Drake, and M. Swisdak, *Physics of Plasmas* **23**, 120704 (2016), arXiv:1607.03857 [physics.plasm-ph].
- ²⁶C. Cattell, J. Dombek, J. Wygant, J. F. Drake, M. Swisdak, M. L. Goldstein, W. Keith, A. Fazakerley, M. André, E. Lucek, and A. Balogh, *J. Geophys. Res.* **110**, A01211 (2005).
- ²⁷J. F. Drake, M. Swisdak, and R. Fermo, *ApJ Lett.* **763**, L5 (2013), arXiv:1210.4830 [astro-ph.SR].
- ²⁸D. Ball, L. Sironi, and F. Özel, *ApJ* **862**, 80 (2018), arXiv:1803.05556 [astro-ph.HE].
- ²⁹F. Guo, Y.-H. Liu, W. Daughton, and H. Li, *ApJ* **806**, 167 (2015), arXiv:1504.02193 [astro-ph.HE].
- ³⁰G. D. Holman, L. Sui, R. A. Schwartz, and A. G. Emslie, *Astrophys. J.* **595**, L97 (2003).
- ³¹L. A. Fisk and G. Gloeckler, *ApJ* **640**, L79 (2006).
- ³²E. C. Stone, A. C. Cummings, F. B. McDonald, B. C. Heikkila, N. Lal, and W. R. Webber, *Nature* **454**, 71 (2008).
- ³³R. B. Decker, S. M. Krimigis, E. C. Roelof, and M. E. Hill, in *Pickup ions throughout the heliosphere and beyond: Proceeding of the 9th international astrophysics conference*, Vol. 1302 (2010) p. 51.

- ³⁴G. P. Zank, P. Hunana, P. Mostafavi, J. A. Le Roux, G. Li, G. M. Webb, O. Khabarova, A. Cummings, E. Stone, and R. Decker, *ApJ* **814**, 137 (2015).
- ³⁵P. Montag, J. Egedal, E. Lichko, and B. Wetherton, *Physics of Plasmas* **24**, 062906 (2017).
- ³⁶X. Li, F. Guo, H. Li, and S. Li, *ApJ* **866**, 4 (2018), arXiv:1807.03427 [astro-ph.SR].
- ³⁷E. P. Kontar, N. H. Bian, A. G. Emslie, and N. Vilmer, *ApJ* **780**, 176 (2014), arXiv:1312.0266 [astro-ph.SR].
- ³⁸M. Onofri, H. Isliker, and L. Vlahos, *Phys. Rev. Lett.* **96**, 151102 (2006).
- ³⁹J. Birn, M. F. Thomsen, and M. Hesse, *Annales Geophysicae* **22**, 1305 (2004).
- ⁴⁰G. Kowal, E. M. de Gouveia Dal Pino, and A. Lazarian, *ApJ* **735**, 102 (2011), arXiv:1103.2984 [astro-ph.HE].
- ⁴¹S. E. Guidoni, C. R. DeVore, J. T. Karpen, and B. J. Lynch, *ApJ* **820**, 60 (2016), arXiv:1603.01309 [astro-ph.SR].
- ⁴²G. Tóth, X. Jia, S. Markidis, I. B. Peng, Y. Chen, L. K. S. Daldorff, V. M. Tenishev, D. Borovikov, J. D. Haiducek, T. I. Gombosi, A. Glocer, and J. C. Dorelli, *Journal of Geophysical Research (Space Physics)* **121**, 1273 (2016).
- ⁴³G. Lapenta, J. U. Brackbill, and P. Ricci, *Physics of Plasmas* **13**, 055904 (2006).
- ⁴⁴M. A. Shay, J. F. Drake, B. N. Rogers, and R. E. Denton, *Geophys. Res. Lett.* **26**, 2163 (1999).
- ⁴⁵M. A. Shay, J. F. Drake, and M. Swisdak, *Phys. Rev. Lett.* **99**, 155002 (2007).
- ⁴⁶H. Karimabadi, W. Daughton, and J. Scudder, *Geophys. Res. Lett.* **34**, L13104 (2007).
- ⁴⁷A. Bhattacharjee, Y.-M. Huang, H. Yang, and B. Rogers, *Physics of Plasmas* **16**, 112102 (2009), arXiv:0906.5599 [physics.plasm-ph].
- ⁴⁸P. A. Cassak, M. A. Shay, and J. F. Drake, *Physics of Plasmas* **16**, 120702 (2009).
- ⁴⁹Y.-M. Huang and A. Bhattacharjee, *Physics of Plasmas* **17**, 062104 (2010), arXiv:1003.5951 [physics.plasm-ph].
- ⁵⁰P. L. Pritchett and F. V. Coroniti, *J. Geophys. Res.* **109**, A01220 (2004).
- ⁵¹J. F. Drake, M. A. Shay, W. Thongthai, and M. Swisdak, *Phys. Rev. Lett.* **94**, 095001 (2005).
- ⁵²Y. Lin and L. C. Lee, *Space Sci. Rev.* **65**, 59 (1993).
- ⁵³C. Z. Cheng, *J. Geophys. Res.* **96**, 21 (1991).

- ⁵⁴W. Park, S. Parker, H. Biglari, M. Chance, L. Chen, C. Z. Cheng, T. S. Hahm, W. W. Lee, R. Kulsrud, D. Monticello, L. Sugiyama, and R. White, *Physics of Fluids B* **4**, 2033 (1992).
- ⁵⁵R. M. Kulsrud, in *Basic Plasma Physics: Selected Chapters, Handbook of Plasma Physics, Volume 1*, edited by A. A. Galeev and R. N. Sudan (1983) p. 1.
- ⁵⁶X.-N. Bai, D. Caprioli, L. Sironi, and A. Spitkovsky, *ApJ* **809**, 55 (2015), arXiv:1412.1087 [astro-ph.HE].
- ⁵⁷C. Tronci, E. Tassi, E. Camporeale, and P. J. Morrison, *Plasma Physics and Controlled Fusion* **56**, 095008 (2014), arXiv:1403.2773 [physics.plasm-ph].
- ⁵⁸E. N. Parker, *Planet Space Sci.* **13**, 9 (1965).
- ⁵⁹X. Li, F. Guo, H. Li, and J. Birn, *ApJ* **855**, 80 (2018), arXiv:1801.02255 [physics.plasm-ph].
- ⁶⁰T. G. Northrop, *Reviews of Geophysics and Space Physics* **1**, 283 (1963).
- ⁶¹H. Nakajima, M. Nishio, S. Enome, K. Shibasaki, T. Takano, Y. Hanaoka, C. Torii, H. Sekiguchi, T. Bushimata, S. Kawashima, N. Shinohara, Y. Irimajiri, H. Koshiishi, T. Kosugi, Y. Shiomi, M. Sawa, and K. Kai, *IEEE Proceedings* **82**, 705 (1994).
- ⁶²D. E. Gary, B. Chen, B. R. Dennis, G. D. Fleishman, G. J. Hurford, S. Krucker, J. M. McTiernan, G. M. Nita, A. Y. Shih, S. M. White, and S. Yu, *ApJ* **863**, 83 (2018), arXiv:1807.02498 [astro-ph.SR].
- ⁶³E. N. Parker, *ApJ* **128**, 664 (1958).
- ⁶⁴M. A. Shay, J. F. Drake, M. Swisdak, W. Dorland, and B. N. Rogers, *Geophys. Res. Lett.* **30**, 1345, doi:10.1029/2002GL016267 (2003).
- ⁶⁵A. Zeiler, D. Biskamp, J. F. Drake, B. N. Rogers, M. A. Shay, and M. Scholer, *J. Geophys. Res.* **107**, 1230 (2002), doi:10.1029/2001JA000287.
- ⁶⁶M. A. Shay, C. C. Haggerty, T. D. Phan, J. F. Drake, P. A. Cassak, P. Wu, M. Oieroset, M. Swisdak, and K. Malakit, *Physics of Plasmas* **21**, 122902 (2014), arXiv:1410.1206 [physics.plasm-ph].
- ⁶⁷C. C. Haggerty, M. A. Shay, J. F. Drake, T. D. Phan, and C. T. McHugh, *Geophys. Res. Lett.* **42**, 9657 (2015), arXiv:1504.02110 [physics.space-ph].
- ⁶⁸J. Egedal, W. Fox, N. Katz, M. Porkolab, M. Øieroset, R. P. Lin, W. Daughton, and J. F. Drake, *Journal of Geophysical Research (Space Physics)* **113**, A12207 (2008).

⁶⁹J. Egedal, W. Daughton, and A. Le, *Nature Physics* **8**, 321 (2012).